International Journal of Multiphase Flow 37 (2011) 241–251

Contents lists available at ScienceDirect

International Journal of Multiphase Flow

journal homepage: www.elsevier.com/locate/ijmulflow

Terminal velocity of a Taylor drop in a vertical pipe

K. Hayashi *, R. Kurimoto, A. Tomiyama

Graduate School of Engineering, Kobe University, 1-1, Rokkodai, Nada, Kobe 657-8501, Japan

ARTICLE INFO

Article history:
Received 17 June 2010
Received in revised form 29 October 2010
Accepted 31 October 2010
Available online 5 November 2010

Keywords:
Taylor drop
Taylor bubble
Terminal velocity
Interface tracking method

ABSTRACT

A scaling analysis based on the field equations for two phases and the jump conditions at the interface is carried out to deduce a balance of forces acting on a Taylor drop rising through stagnant liquid in a vertical pipe. The force balance is utilized to deduce a functional form of an empirical correlation of terminal velocity of the Taylor drop. Undetermined coefficients in the correlation are evaluated by making use of available correlations for two limiting cases, i.e. extremely high and low Reynolds number Taylor bubbles in large pipes. Terminal velocity data obtained by interface tracking simulations are also used to determine the coefficients. The proposed correlation expresses the Froude number Fr as a function of the drop Reynolds number Re_D, the Eötvös number Eo_D and the viscosity ratio μ^*. Comparisons between the correlation, simulations and experimental data confirm that the proposed correlation is applicable to Taylor drops under various conditions, i.e., $0.002 < Re_D < 4960$, $4.8 < Eo_D < 228$, $0 \leqslant \mu^* \leqslant 70$, $1 < N < 14700$, $-12 < \log M < 4$, and $d/D < 1.6$, where N is the inverse viscosity number, M the Morton number, d the sphere-volume equivalent drop diameter and D the pipe diameter.

1. Introduction

Large gas bubbles in gas–liquid two-phase slug flows in vertical pipes take bullet shapes. They are called Taylor bubbles (Davies and Taylor, 1950). Since large drops in vertical pipes also take bullet shapes, they can be also referred to as Taylor drops.

Many studies have been carried out on the motion of a Taylor bubble, and various models for the terminal velocity, V_T, have been proposed. A review and comparisons between available V_T models for a Taylor bubble can be found in literature (Viana et al., 2003). Since the viscosity of the gas phase has no influence on V_T, these V_T models do not take into account the bubble viscosity. On the other hand, the drop viscosity affects V_T of the Taylor drop.

In contrast to the Taylor bubble, there are few studies on the Taylor drop. Goldsmith and Mason (1962) deduced a V_T model for Taylor drops at low drop Reynolds numbers, Re_D, in which the effects of the drop viscosity on V_T were accounted for. The original expression of Goldsmith's V_T model can be rearranged as follows:

$$V_T = \left[\frac{f_1 - 1 + (f_1 f_2 - f_3)(\mu_D/\mu_C)}{1 + f_2(1 + f_2/4)(\mu_D/\mu_C)}\right]\frac{\Delta\rho g D^2}{\mu_C} \tag{1}$$

$$f_1 = \frac{(R-h)^2}{8R^2}\left[\frac{R^2 - (R-h)^2}{2(R-h)^2} - \ln\left(\frac{h}{R-h}\right)\right]$$

$$f_2 = 2\left[\left(\frac{R}{R-h}\right)^2 - 1\right]$$

$$f_3 = 4\ln\left(\frac{R}{R-h}\right)$$

where $\Delta\rho$ ($=\rho_C - \rho_D$) is the density difference between the two phases, ρ the density, g the magnitude of the acceleration of gravity, D the pipe diameter, μ the viscosity, and f_i (i = 1–3) are functions of the pipe radius, R, and the thickness, h, of the liquid film between the drop and the pipe wall. The subscripts, C and D, denote the continuous and dispersed phases, respectively. The drop Reynolds number is defined by

$$Re_D = \frac{\rho_C V_T D}{\mu_C} \tag{2}$$

Eq. (1) can be further rewritten in the following non-dimensional form:

$$Fr = \left[\frac{f_1 - 1 + (f_1 f_2 - f_3)\mu^*}{1 + f_2(1 + f_2/4)\mu^*}\right]N \tag{3}$$

where Fr is the Froude number, N is referred to as the inverse viscosity number or the Archimedes number, and μ^* is the viscosity ratio:

$$Fr = \frac{V_T}{\sqrt{\Delta\rho g D/\rho_C}} \tag{4}$$

* Corresponding author. Tel./fax: +81 78 803 6108.
E-mail address: hayashi@mech.kobe-u.ac.jp (K. Hayashi).

0301-9322/$ - see front matter © 2010 Elsevier Ltd. All rights reserved.
doi:10.1016/j.ijmultiphaseflow.2010.10.008

$$N = \frac{\sqrt{\rho_C \Delta\rho g D^3}}{\mu_C} \tag{5}$$

$$\mu^* = \frac{\mu_D}{\mu_C} \tag{6}$$

They also carried out experiments of Taylor drops and confirmed the validity of their model.

Mandal et al. (2007) measured terminal velocities of Taylor drops at high Re_D for various fluids. They confirmed that the terminal velocity can be evaluated by using the following V_T model for spherical-cap bubbles in infinite stagnant liquids (Joseph, 2003):

$$Fr = -\frac{8}{3}\frac{(1+8s)}{N} + \frac{\sqrt{2}}{3}\sqrt{1 - 2s + \frac{16s}{Eo_D} + \frac{32}{N^2}(1+8s)^2} \tag{7}$$

where s is the deviation of the interface from perfect sphericity near the nose of a bubble, and Eo_D is the Eötvös number defined by

$$Eo_D = \frac{\Delta\rho g D^2}{\sigma} \tag{8}$$

where σ is the surface tension. Their work implies that V_T of a Taylor drop at high Re_D is independent of μ^*. Mandal et al. (2009) recently proposed another correlation of V_T, which is a combination of Brown's Fr model (Brown, 1965) and a function of Eo_D used in Viana's correlation for a Taylor bubble (Viana et al., 2003). Since the effect of μ^* is not taken into account, this model is also applicable only to drops at high Re_D.

These models, Eqs. (3) and (7), are applicable only to the viscous force dominant (low Re_D) regime and to the inertial force dominant (high Re_D) regime, respectively. In addition, without the knowledge on the drop shape parameters, h and s, they are of no use.

The purpose of this study is to develop a Fr correlation for Taylor drops. A Fr correlation for Taylor bubbles has been already developed by the authors (Hayashi et al., 2010) by making use of a scaling analysis based on the local instantaneous field equations and the jump conditions at the interface (Tomiyama, 2004). By introducing the effect of μ^* into the correlation, the correlation is extended so as to be applicable to Taylor drops. Coefficients in the extended correlation are determined using a database of Froude numbers obtained by using an interface tracking method (Hayashi et al., 2006; Hayashi and Tomiyama, 2007, 2009). Experiments of Taylor drops are also carried out to examine the validity of the interface tracking simulation.

2. Scaling analysis

2.1. Derivation of functional form of Fr

The field equations and the jump conditions for incompressible viscous fluids at steady state are given by

$$\nabla \cdot \mathbf{V}_k = 0 \tag{9}$$

$$\mathbf{V}_k \cdot \nabla \mathbf{V}_k = -\frac{1}{\rho_k}\nabla P_k + \mathbf{g} + \frac{1}{\rho_k}\nabla \cdot \tau_k \tag{10}$$

$$(\mathbf{V}_D - \mathbf{V}_C) \cdot \mathbf{n} = 0 \tag{11}$$

$$-(P_D - P_C - \kappa\sigma)\mathbf{n} + (\tau_D - \tau_C) \cdot \mathbf{n} = 0 \tag{12}$$

where the subscript k denotes the phase ($k = D$ and C for the dispersed and continuous phases, respectively), $\boldsymbol{V}$ is the velocity, P the pressure, $\boldsymbol{g}$ the acceleration of gravity, τ the viscous stress tensor, $\boldsymbol{n}$ the unit normal to the interface, and κ the curvature. Terminal velocities of small and Taylor drops in vertical pipes have been measured by Kurimoto et al. (2010), which show that the terminal velocity of the Taylor drop depends on the pipe diameter D but not on the drop length at least for $d/D < 1.6$, where d is the sphere-volume equivalent drop diameter. Taylor drops only in the same range of d/D are dealt with in this study. Hence the characteristic length, velocity, and time scales for the problem of concern are D, V_T and D/V_T, respectively. As shown in Fig. 1, the orders of magnitude of the viscous stress tensors can be estimated as

$$\tau_D \cong \mu_D \frac{V_T + V_i}{R - h} \tag{13}$$

$$\tau_C \cong \mu_C \frac{V_i}{h} \tag{14}$$

where V_i is the interfacial velocity. Since it is difficult to estimate V_i, Eqs. (13) and (14) are rewritten as follows by introducing functions, C_{D1} and C_{C1}, which implicitly include the effect of V_i:

$$\tau_D \cong C_{D1}\mu_D \frac{V_T}{R - h} \tag{15}$$

$$\tau_C \cong C_{C1}\mu_C \frac{V_T}{h} \tag{16}$$

Substituting Eqs. (15) and (16) and the characteristic scales into Eq. (10) yields

$$P_D \cong C_{D1}\mu_D V_T D/(R-h)^2 + C_{D2}\rho_D V_T^2 + C_{D3}\rho_D g D \tag{17}$$

$$P_C \cong C_{C1}\mu_C V_T D/h^2 + C_{C2}\rho_C V_T^2 + C_{C3}\rho_C g D \tag{18}$$

where C_{ki} ($k = D$ or C and $i = 1, 2, 3$) are functions of relevant dimensionless groups and they can be constant in some limiting cases. The curvature, κ, in Eq. (12) is estimated as

$$\kappa \cong 1/(R-h) \tag{19}$$

Substituting Eqs. (17)–(19) into Eq. (12) gives the following force balance:

$$C_1\rho_C V_T^2 D^2 + C_2\rho_D V_T^2 D^2 + C_3\mu_C V_T \frac{D^3}{h^2} + C_4\mu_D V_T \frac{D^3}{(R-h)^2} + C_5\sigma\frac{D^2}{R-h} + C_6\Delta\rho g D^3 = 0 \tag{20}$$

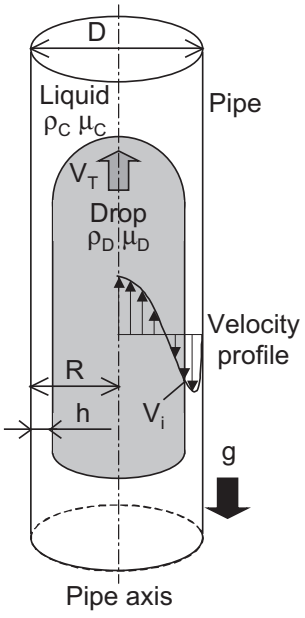

Fig. 1. Large drop in a pipe.

where C_i (i = 1–6) are coefficients consisting of C_{ki}. This equation indicates that the six different forces, i.e., inertial (F_{iC} and F_{iD}), viscous ($F_{\mu C}$ and $F_{\mu D}$), surface tension (F_s) and buoyant (F_b) forces, govern the dynamics of a Taylor drop. The relevant dimensionless groups, Fr, N, Eo_D, M, Re_D, ρ^* and μ^*, are represented by using these forces:

$$Fr = \sqrt{\frac{F_{iC}}{F_b}} = \frac{V_T}{\sqrt{\Delta\rho g D/\rho_C}} \quad \text{(Froude number)} \tag{21}$$

$$N = \sqrt{\frac{F_{iC}F_b}{F_{\mu C}^2}} = \frac{\sqrt{\rho_C \Delta\rho g D^3}}{\mu_C} \quad \text{(inverse viscosity number)} \tag{22}$$

$$Eo_D = \frac{F_b}{F_s} = \frac{\Delta\rho g D^2}{\sigma} \quad \text{(Eötvös number)} \tag{23}$$

$$M = \frac{F_{\mu C}^4 F_b}{F_s^3 F_{iC}^2} = \frac{g\mu_C^4 \Delta\rho}{\rho_C^2 \sigma^3} \quad \text{(Morton number)} \tag{24}$$

$$Re_D = \frac{F_{iC}}{F_{\mu C}} = \frac{\rho_C V_T D}{\mu_C} \quad \text{(drop Reynolds number)} \tag{25}$$

$$\rho^* = \frac{F_{iD}}{F_{iC}} = \frac{\rho_D}{\rho_C} \quad \text{(density ratio)} \tag{26}$$

$$\mu^* = \frac{F_{\mu D}}{F_{\mu C}} = \frac{\mu_D}{\mu_C} \quad \text{(viscosity ratio)} \tag{27}$$

Only five independent dimensionless groups can be deduced from the six forces. Furthermore the constraint given by Eq. (20) reduces the number of independent dimensionless groups from five to four. By selecting Re_D, Eo_D, ρ^* and μ^* as the four independent variables, we can obtain the following fundamental functional form of Fr from Eq. (20):

$$Fr = \sqrt{\frac{c_1\left(\frac{h}{D}\right)^2\left(1 + c_5\frac{D}{R-h}\frac{1}{Eo_D}\right)}{\left(\frac{h}{D}\right)^2(c_2 + c_3\rho^*) + \frac{1}{Re_D}\left(1 + c_4\frac{h^2}{(R-h)^2}\mu^*\right)}} \tag{28}$$

where c_i (i = 1–5) are undetermined coefficients given by $c_1 = -C_6/C_3$, $c_2 = C_1/C_3$, $c_3 = C_2/C_3$, $c_4 = C_4/C_3$, and $c_5 = C_5/C_6$. The effects of μ^* vanish when the Re_D is much larger than the factor including μ^*. As described above, the viscosity ratio does not affect Fr at high Re_D (Mandal et al., 2007). Hence the functional form of Eq. (28) is reasonable with respect to the μ^* dependency.

The scaling analysis does not give the values of the coefficients in Eq. (28). Hence the coefficients must be determined using the knowledge on Fr.

2.2. Fr correlation for Taylor bubbles

It can be postulated for a bubble in a liquid that $\rho^* \approx 0$ and $\mu^* \approx 0$. Then Eq. (28) simplifies to

$$Fr = \sqrt{\frac{c_1\left(\frac{h}{D}\right)^2}{c_2\left(\frac{h}{D}\right)^2 + \frac{1}{Re_D}}\left(1 + c_5\frac{D}{(R-h)}\frac{1}{Eo_D}\right)} \tag{29}$$

Let us consider two limiting cases, i.e., the inertial force dominant ($Re_D \to \infty$ and $Eo_D \to \infty$) and the viscous force dominant ($Re_D \to 0$ and $Eo_D \to \infty$) cases to determine the coefficients, c_1 and c_2, in Eq. (29). In the former case, Eq. (29) reduces to

$$Fr = \sqrt{\frac{c_1}{c_2}} \tag{30}$$

Since the Froude number in the inertial force dominant regime is known to be 0.35 (Brown, 1965; Collins et al., 1978; Dumitrescu, 1943; Griffith and Wallis, 1961; Harmathy, 1960; Wallis, 1969; White and Beardmore, 1962), we obtain

$$\sqrt{\frac{c_1}{c_2}} = 0.35 \tag{31}$$

Substituting a relation, $Re_D = FrN$, into Eq. (29) yields

$$c_2\left(\frac{h}{D}\right)^2 Fr^2 + \frac{Fr}{N} = c_1\left(\frac{h}{D}\right)^2\left(1 + c_5\frac{D}{(R-h)}\frac{1}{Eo_D}\right) \tag{32}$$

According to Wallis (1969), Fr of a Taylor bubble in the viscous force dominant regime is given by

$$Fr = 0.01N \tag{33}$$

Substituting the above equation into Eq. (32) and taking the limit $Eo_D \to \infty$ yields

$$c_2\left(\frac{h}{D}\right)^2 Fr^2 + 0.01 = c_1\left(\frac{h}{D}\right)^2 \tag{34}$$

Since Fr vanishes at $Re_D \to 0$, Eq. (34) reduces to

$$c_1\left(\frac{h}{D}\right)^2 = 0.01 \tag{35}$$

From Eqs. (31) and (35)

$$c_2\left(\frac{h}{D}\right)^2 = 0.0816 \tag{36}$$

Substituting Eqs. (35) and (36) into Eq. (29) yields

$$Fr = \sqrt{\frac{0.01}{0.0816 + \frac{1}{Re_D}}G} \tag{37}$$

where

$$G = 1 + c_5\frac{D}{R-h}\frac{1}{Eo_D} \tag{38}$$

Then, taking the limit, $Eo_D \to \infty$, in Eq. (37) gives

$$Fr = \sqrt{\frac{0.01}{0.0816 + \frac{1}{Re_D}}} \tag{39}$$

Since the above equation is derived by making use of the two limiting cases, $Re_D \to \infty$ and $Re_D \to 0$, its applicability to intermediate Reynolds numbers should be tested against experimental data of high Eötvös numbers, $Eo_D > 100$. As shown in Fig. 2, Eq. (39) agrees well with the experimental data (White and Beardmore, 1962; Wallis, 1969) not only at high and low Reynolds numbers, $Re_D > 10^3$ and $Re_D < 1$, but also at intermediate Reynolds numbers, $1 < Re_D < 10^3$.

Then the remaining term to be determined in Eq. (37) is G. This term might be a function of two dimensionless groups, e.g., Re_D and Eo_D. As can be understood from Eq. (38), the most relevant dimensionless number is, of course, the Eötvös number. Hence, for simplicity, let us deduce an empirical correlation of G in terms of Eo_D. Solving Eq. (37) for G gives

$$G = \left(\frac{Fr}{0.1}\right)^2\left(0.0816 + \frac{1}{Re_D}\right) \tag{40}$$

Fig. 3 shows the values of G obtained by substituting White and Beardmore's data (1962) into the above equation. Though there is a small scatter in the data, G is well correlated with the following function:

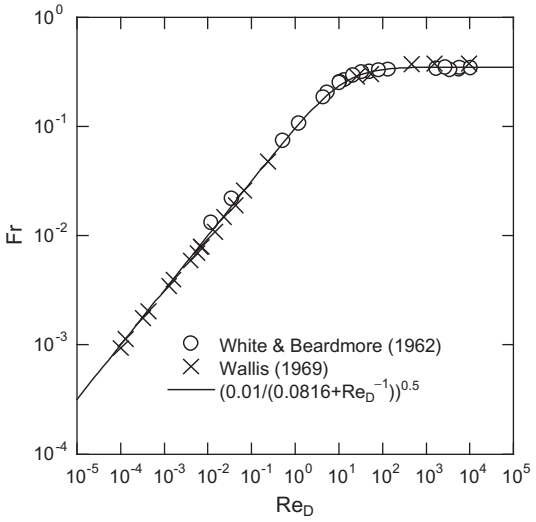

Fig. 2. Relation between Re_D and Fr for $Eo_D > 100$.

$$G = \left(1 + \frac{41}{Eo_D^{1.96}}\right)^{-4.63} \tag{41}$$

By substituting Eq. (41) into Eq. (37), we obtain the following correlation of Fr for Taylor bubbles:

$$Fr = \sqrt{\frac{0.01}{0.0816 + Re_D^{-1}}\left(1 + \frac{41}{Eo_D^{1.96}}\right)^{-4.63}} \tag{42}$$

Substituting the relations, $Re_D = FrN$ and $N = (Eo_D^3/M)^{1/4}$, into Eq. (42) yields

$$0.0816Fr^2 + \frac{M^{1/2}}{Eo_D^{3/4}}Fr = 0.01\left(1 + \frac{41}{Eo_D^{1.96}}\right)^{-4.63} \tag{43}$$

By taking the limit $M \to 0$, the above equation reduces to

$$Fr = 0.35\left(1 + \frac{41}{Eo_D^{1.96}}\right)^{-2.32} \tag{44}$$

This simplified equation is applicable to low viscosity systems such as vapor bubbles in water. It should be noted that the three limits, $Re_D \to \infty$, $N \to \infty$ and $M \to 0$, lead to the same limiting case. Comparisons between Eq. (44) and available correlations for Taylor bubbles for $\log M < -7.7$ (Wallis, 1969; Tung and Parlange, 1976; Nickens and Yannitell, 1987; Viana et al., 2003) are shown in Fig. 4. Eq. (44) is much better than Wallis', Tung's and Nickens' correlations and is comparable with Viana's correlation.

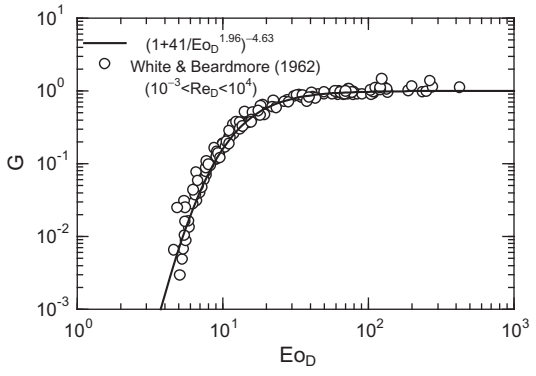

Fig. 3. Function G.

Eq. (42) agrees with most of Fr data obtained by White and Beardmore (1962) to within ±10% errors (Hayashi et al., 2010). The accuracy is, however, not so good at intermediate Morton numbers. This shortcoming can be overcome by introducing a correction into Eq. (42) while taking into account the nonlinear effects, e.g.,

$$Fr = \sqrt{\frac{0.0089}{0.0725 + \frac{1}{Re_D}\left(1 - 0.11Re_D^{0.33}\right)}\left(1 + \frac{41}{Eo_D^{1.96}}\right)^{-4.63}} \tag{45}$$

where the values of the coefficients, c_1 and c_2, are also slightly changed to improve the accuracy. This equation is compared with White and Beardmore's experimental data (1962) in Fig. 5. Good agreements between the data and Eq. (45) are obtained for a wide range of the dimensionless groups, Eo_D and M.

The coefficients, c_3 and c_4, in Eq. (28) must be determined based on the knowledge on the effects of ρ^* and μ^* on Fr of Taylor drops. There are, however, no databases of Fr for various values of ρ^* and μ^*. The effects of ρ^* and μ^* on Fr were, therefore, investigated by making use of an interface tracking method.

3. Numerical method

The following mass and momentum equations based on the one-field formulation for an incompressible two-phase flow are adopted (Hirt and Nicholds, 1981; Scardovelli and Zaleski, 2000):

$$\nabla \cdot \mathbf{V} = 0 \tag{46}$$

$$\rho_M\left[\frac{\partial \mathbf{V}}{\partial t} + \mathbf{V} \cdot \nabla \mathbf{V}\right] = -\nabla P + \nabla \cdot \mu_M[\nabla \mathbf{V} + (\nabla \mathbf{V})^T] + \rho \mathbf{g} + \sigma\kappa \mathbf{n}\delta \tag{47}$$

where t is the time, δ the delta function and the superscript T denotes the transpose. The mixture density, ρ_M, is given by

$$\rho_M = (1 - \alpha)\rho_D + \alpha\rho_C \tag{48}$$

where α is the cell-averaged volume fraction of the continuous phase. The harmonic mean of the viscosity should be used rather

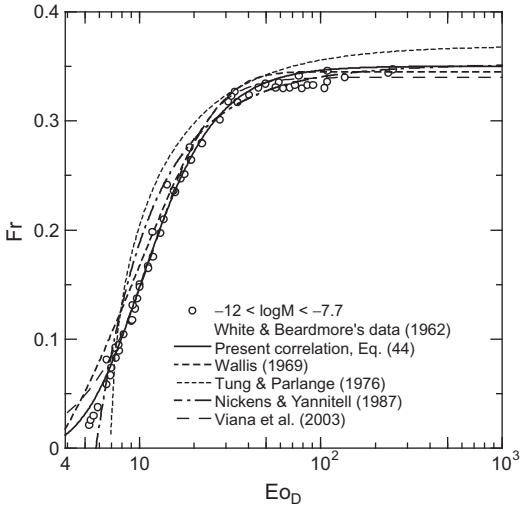

Fig. 4. Comparisons between Eq. (44) and available correlations for Taylor bubbles at low Morton numbers.

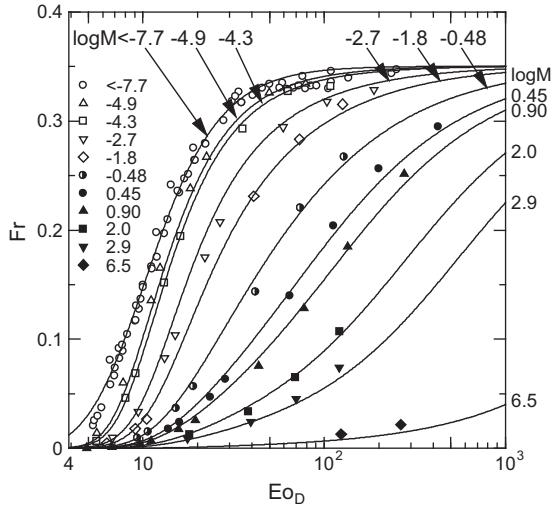

Fig. 5. Comparison between Eq. (45) and White and Beardmore's data (1962).

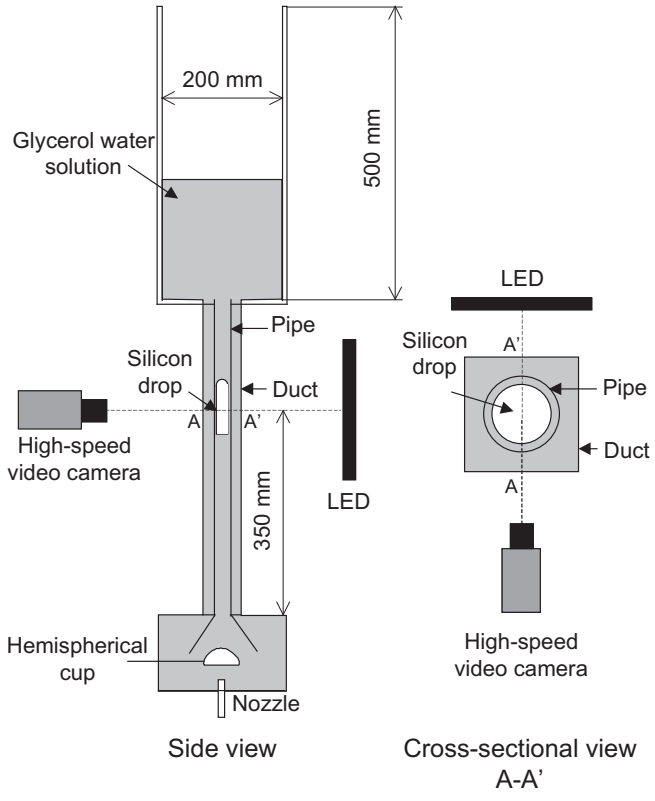

Fig. 6. Experimental apparatus.

than the arithmetic mean to correctly deal with the continuity of the viscous stresses. Hence the mixture viscosity, μ_M, is given by

$$\frac{1}{\mu_M} = \frac{1-\alpha}{\mu_D} + \frac{\alpha}{\mu_C} \tag{49}$$

The density and viscosity of each phase are assumed to be constant. The computational cell is filled with the continuous phase when $\alpha = 1$, and with the dispersed phase when $\alpha = 0$. A cell with $0 < \alpha < 1$ contains an interface. The interface motion is calculated by solving the following advection equation of α:

$$\frac{\partial \alpha}{\partial t} + \nabla \cdot \alpha \mathbf{V} = \alpha \nabla \cdot \mathbf{V} \tag{50}$$

Eqs. (46) and (47) are solved by using the modified SOLA (solution algorithm) (Tomiyama and Hirano, 1994). An interface tracking method based on a volume-of-fluid method, which we call the NSS (non-uniform subcell scheme) (Hayashi et al., 2006), is used to solve Eq. (50). The amount of fluid volumes transferred from an interface cell to its neighbor cells is accurately calculated by making use of non-uniform subcells which are temporarily introduced only in the interface cells. A local level set function is also computed in the interface cells, by which the surface tension force in Eq. (47) is accurately evaluated. The NSS can be implemented not only in Cartesian coordinates but also in cylindrical and general curvilinear coordinates. Since all the Taylor drops dealt with in this study are axisymmetric, the two-dimensional (r, z) cylindrical coordinate system is used. The details of the NSS can be found in Hayashi et al. (2006) and Hayashi and Tomiyama (2007, 2009).

4. Validation

4.1. Experimental setup

Terminal velocities and shapes of single Taylor drops were measured to obtain experimental data for comparisons with simulations. The experiments were carried out at atmospheric pressure and room temperature (the temperature of the liquid and drops were kept at 298 ± 0.5 K). The experimental apparatus is shown in Fig. 6. It consists of the vertical pipe and the square tanks. Four pipes of D = 11.0, 20.1, 26.1 and 30.8 mm were used to alter the values of Eo_D. The pipe length was 530 mm. The pipes and the tanks were made of transparent acrylic resin.

Silicon oils of various viscosities (Sin-etsu silicon, KF96-10, 30, 100, 300, 500, 1000 and KF96-5000) and glycerol-water solutions were used for the dispersed and continuous phases, respectively. The density, viscosity, surface tension and temperature were measured using a densimeter (Ando Keiki Co., Ltd., JIS B7525), a viscometer (Rion Co., Ltd., Viscotester VT-03E), capillary tubes (glass tube, 1.02 mm i.d.) and a digital thermometer (Sato Keiryoki MFG. Co., Ltd., SK-1250MC), respectively. Fluid properties were

Table 1
Experimental conditions.

Case	1	2	3	4	5	6	7	8	9	10	11	12	13	14
ρ_C (kg/m^3)	1220	1220	1220	1190	1190	1190	1240	1240	1240	1240	1240	1240	1240	1240
ρ_D (kg/m^3)	955	965	970	935	955	965	915	935	955	965	970	970	970	975
μ_C (mPa·s)	85	85	85	25	25	25	262	262	262	262	262	262	262	262
μ_D (mPa·s)	29	97	485	9.4	29	97	4.6	9.4	29	97	291	485	970	4875
σ (mN/m)	31	31	31	38	32	37	29	29	29	29	28	28	29	28
D (mm)	11, 20, 26, 31				11, 20, 26					11, 20, 31				
log$M$	−2.5				−4.7					−0.45				
ρ^*	0.78	0.79	0.80	0.79	0.80	0.81	0.74	0.75	0.77	0.78	0.78	0.78	0.78	0.79
μ^*	0.34	1.1	5.7	0.37	1.1	3.8	0.02	0.04	0.11	0.37	1.1	1.9	3.7	19
Eo_D	≈10, 33, 55, 77				≈ 8, 26, 44					≈ 12, 39, 91				

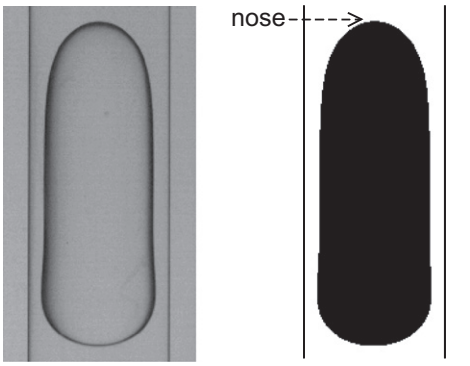

Fig. 7. Raw and binary images of a Taylor drop.

measured at least five times. Uncertainties estimated at 95% confidence in measured ρ, μ and σ were 0.021%, 0.53% and 4.0%, respectively. The measured values of these fluid properties agreed well with the data given in literature (Ishikawa, 1968). The values in literature were, therefore, used in calculations of the dimensionless numbers and in numerical simulations. Fluid systems used in the present experiments are summarized in Table 1. The ranges of dimensionless groups were $7.2 < Eo_D < 92$, $7.9 < N < 270$, $-4.7 < \log M < -0.4$, $0.017 < \mu^* < 19$, and $0.74 < \rho^* < 0.81$.

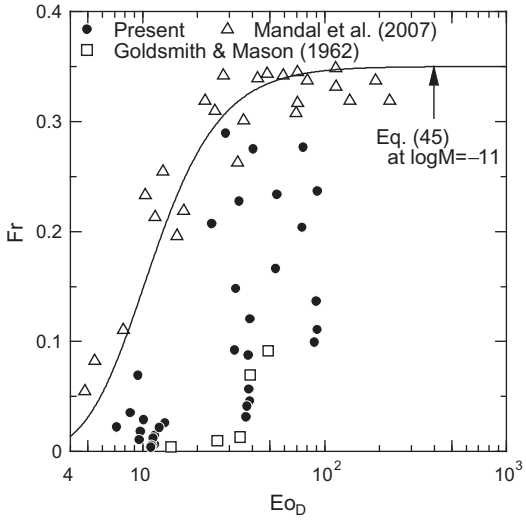

Fig. 8. Froude numbers measured in the present study and *Fr* data collected from literature (Goldsmith and Mason, 1962; Mandal et al., 2007).

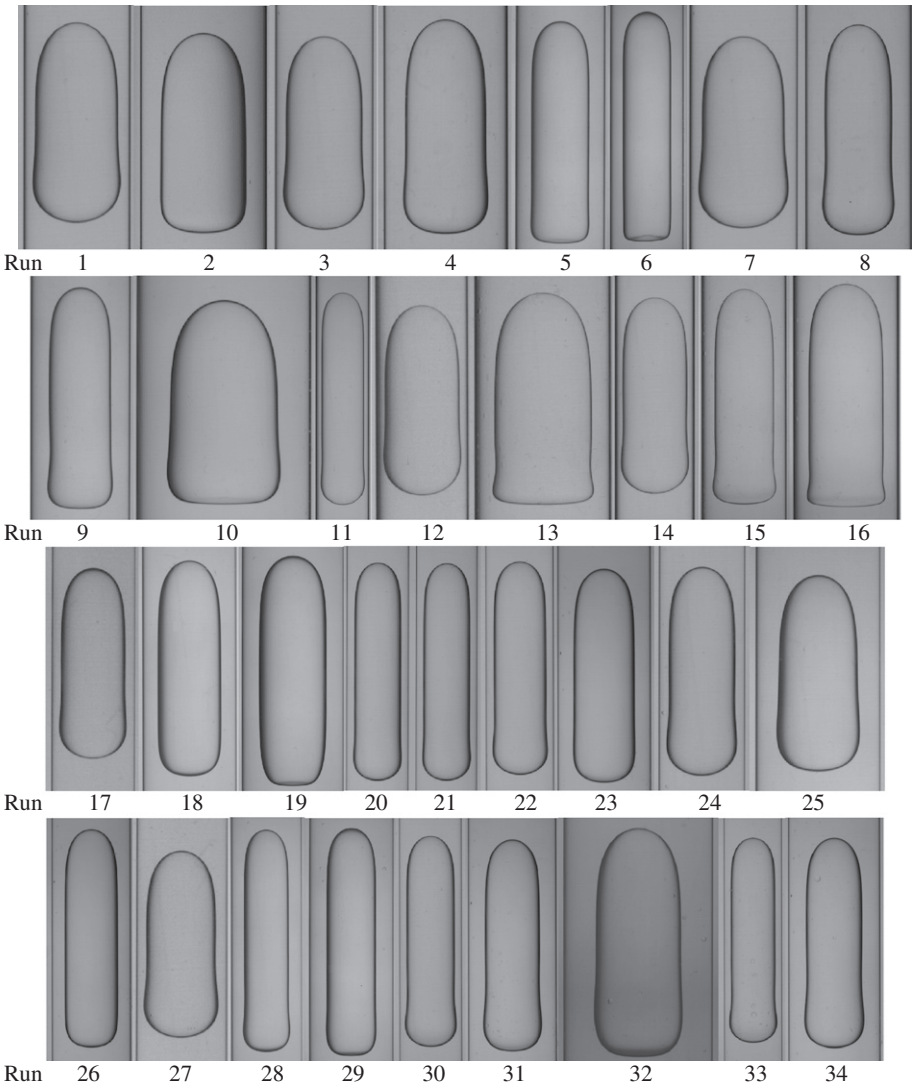

Fig. 9. Drop shapes.

A small amount of silicon oil was stored in the hemispherical glass cup. A single drop was released by rotating the cup. The visualization of the drop motion and shape using a high-speed video camera (Integrated Design Tools Inc., Motionscope M3, frame rate = 20–400 frame/s, spatial resolution ≈0.095 mm/pixel) confirmed that drops were axisymmetric and rose rectilinearly along the pipe axis.

Successive images of drops in the pipe were taken by using the high-speed video camera at 350 mm above the bottom of the pipe to obtain experimental data only at terminal conditions. The length of the measuring section was 120 mm. It took over 2 s for all the drops to pass through the measuring section. The frame rate of the high-speed video camera was adjusted to a value for obtaining 1000 images for each drop. The pipe was enclosed with the acrylic duct. The gap between the pipe and the duct was filled with the same glycerol-water solution as that in the pipe to reduce optical distortion of drop images. A LED light source (Hayashi Watch-Works, LP-2820) was used for back illumination.

The sphere-volume equivalent diameters, d, of drops were calculated from the drop images using an image processing method (Tomiyama et al., 2002). An example of drop images is shown in Fig. 7. The instantaneous velocity of a drop was computed by measuring the difference in elevation of the noses of two consecutive drop images. Time series of the drop velocity was obtained by processing the 1000 images. Drop velocities were constant while a drop rose through the measuring section. Hence the drops reached their terminal conditions at the measuring section.

4.2. Experimental results

All the Fr data and drop shapes obtained by 34 runs are shown in Figs. 8 and 9. The values of Fr and drop shapes are given in Table 2. The experimental data obtained by Goldsmith and Mason (1962) and Mandal et al. (2007) are also plotted in the figure. Goldsmith and Mason dealt with only low Reynolds number drops, in other words, low Fr drops. The ranges of dimensionless groups examined by them are $14 < Eo_D < 50$, $1 < N < 12$, $\log M = 0.76$ and 3.4, $\mu^* = 0.0012$ and 0.075, $1.2 < \rho^* < 1.5$, $0.004 < Re_D < 1.1$, and $0.004 < Fr < 0.091$. On the other hand, Mandal's experimental data were only for drops in low viscosity systems. The ranges of dimensionless groups are $4.8 < Eo_D < 228$, $1430 < N < 14300$, $-11 < \log M < -9.3$, $0.69 < \mu^* < 1.2$, $0.66 < \rho^* < 0.88$, $78 < Re_D < 4960$, and $0.05 < Fr < 0.349$. Since the drop viscosity dissipates the kinetic energy, Fr may decrease as μ^* increases. However, their data largely scatter and several data exceed the values of Fr evaluated with Eq. (45) at $\log M = -11$. Taylor drops in low viscosity systems and those in large pipes tend to oscillate due to the Rayleigh–Taylor instability. This may be a reason why Mandal's data show a large scatter. Fig. 8 also shows that the present experiments cover a wide range of dimensionless groups, i.e., $7.2 < Eo_D < 92$, $7.9 < N < 270$, $-4.7 < \log M < -0.4$, $0.017 < \mu^* < 19$, $0.74 < \rho^* < 0.81$, $0.029 < Re_D < 74$, and $0.0037 < Fr < 0.284$, and therefore, they fill the gap between Goldsmith's and Mandal's data.

Figs. 10–12 are measured Fr at $\log M = -0.45$, -2.5 and -4.7, respectively. Eq. (45) is also drawn in the figures as the reference case of $\mu^* = 0$. The effects of μ^* on Fr can be understood from these figures: (I) Fr monotonously decreases with increasing μ^*, (II) the influence of μ^* vanishes when μ^* is very small, and (III) μ^* does not have much influence on Fr at low M. The tendency (II) supports the model of Goldsmith and Mason, and the term in the square brackets in Eq. (3) must decrease with increasing μ^* because of the tendency (I). Then the tendency (III) qualitatively agrees with the observation of Mandal et al. that Fr of a drop at low M is independent of μ^*.

The Froude numbers at $Eo_D \simeq 12$, 39 and 91 are plotted against μ^* in Fig. 13 to make clear the effects of μ^*. Fr decreases with increasing μ^*, and the magnitude of the gradient, $dFr/d\mu^*$, decreases as μ^* increases.

Since the density ratio is about 0.8 for all the experiments, the effects of ρ^* cannot be discussed. These are, therefore, investigated by making use of the numerical simulation.

Table 2
Measured Froude numbers.

Run	Eo_D	N	$\log M$	μ^*	Re_D	Fr
1	10	24	−2.5	0.34	0.70	0.029
2	34	60	−2.5	0.34	13.7	0.23
3	9.7	24	−2.5	1.1	0.41	0.017
4	32	58	−2.5	1.1	8.7	0.15
5	55	87	−2.5	1.1	20.2	0.23
6	76	111	−2.5	1.1	31.0	0.28
7	9.6	23	−2.5	5.7	0.21	0.0088
8	32	58	−2.5	5.7	5.3	0.092
9	54	86	−2.5	5.7	13.8	0.16
10	75	110	−2.5	5.7	22.0	0.20
11	9.4	79	−4.9	0.37	6.0	0.075
12	8.6	76	−4.7	1.1	3.1	0.040
13	29	188	−4.7	1.1	55.3	0.29
14	7.2	75	−4.9	3.9	1.2	0.016
15	24	184	−4.9	3.9	36.2	0.20
16	41	273	−4.9	3.9	73.6	0.27
17	12	8.2	−0.45	0.11	0.14	0.017
18	39	20	−0.45	0.11	2.4	0.12
19	91	38	−0.45	0.11	9.04	0.24
20	13	8.8	−0.40	0.017	0.23	0.027
21	12	8.5	−0.44	0.036	0.19	0.022
22	11	8.1	−0.45	0.37	0.096	0.012
23	38	20	−0.45	0.37	1.7	0.086
24	11	8.0	−0.42	1.1	0.064	0.0080
25	38	20	−0.42	1.1	1.2	0.059
26	90	37	−0.42	1.1	5.1	0.14
27	12	20	−0.41	1.9	0.053	0.0067
28	39	37	−0.41	1.9	0.98	0.050
29	91	24	−0.41	1.9	4.3	0.12
30	11	8.0	−0.46	3.7	0.041	0.0051
31	37	20	−0.46	3.7	0.83	0.042
32	88	37	−0.46	3.7	4.0	0.11
33	11	7.9	−0.46	19	0.029	0.0037
34	37	20	−0.46	19	0.71	0.036

4.3. Simulation

Fig. 14 shows a computational domain and the initial condition. The drop was initially set at the center of the computational

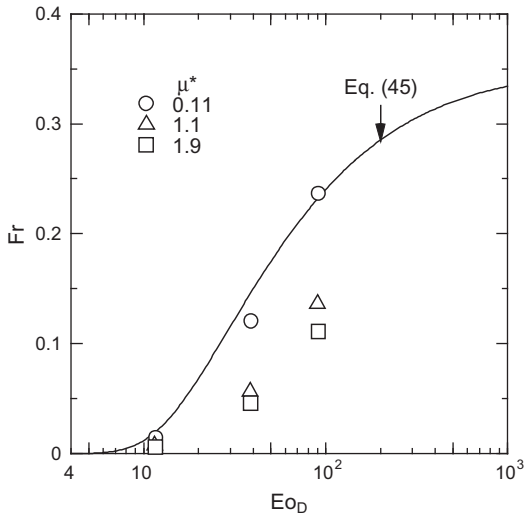

Fig. 10. Froude numbers at $\log M = -0.45$.

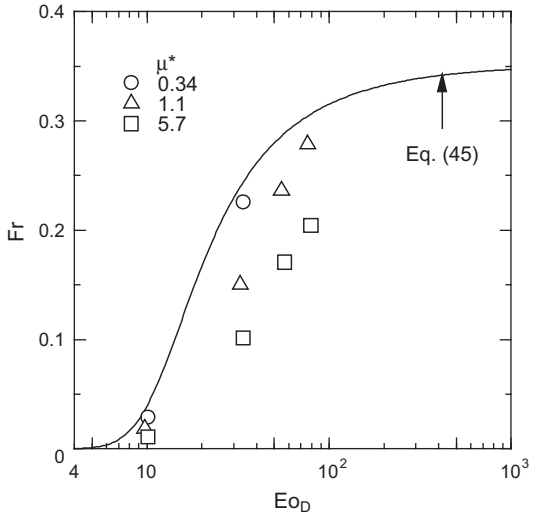

Fig. 11. Froude numbers at $\log M = -2.5$.

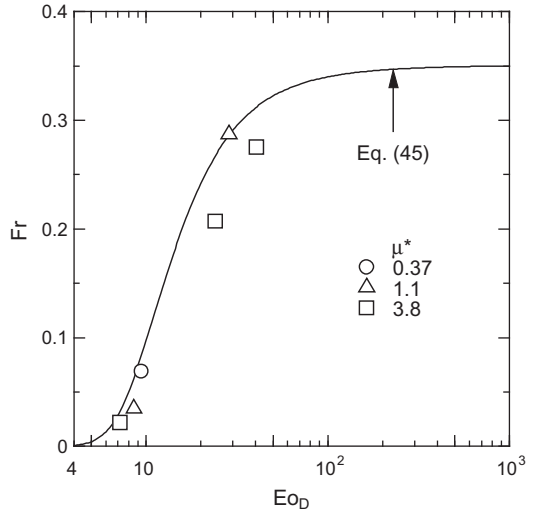

Fig. 12. Froude numbers at $\log M = -4.7$.

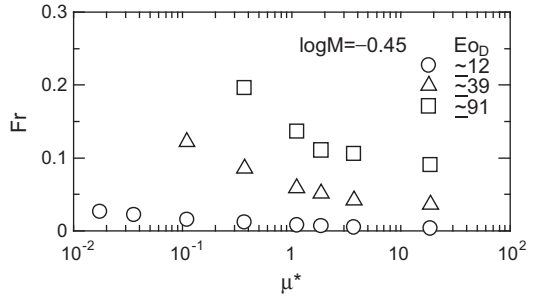

Fig. 13. Froude numbers at various μ^*.

domain. The initial drop shape was a cylinder with two hemispheres attached to the top and bottom of the cylinder. The drop length was L and the thickness, h, of the liquid film was $0.2R$. The ratio of the sphere-volume equivalent diameter, d, to the pipe diameter, D, was 1.25. The domain size was $(R, 4L)$. The top and bottom boundaries were uniform inflow and continuous outflow, respectively. The right boundary was a wall moving downward at the drop terminal velocity. The left was an axisymmetric boundary. Uniform computational cells of $\Delta r = \Delta z = R/32$ were used. The total number of cells was 18,816 (=32 × 588). The time step, Δt, ranged from 1×10^{-3} to 1×10^{-2} ms which satisfied the condition of numerical stability.

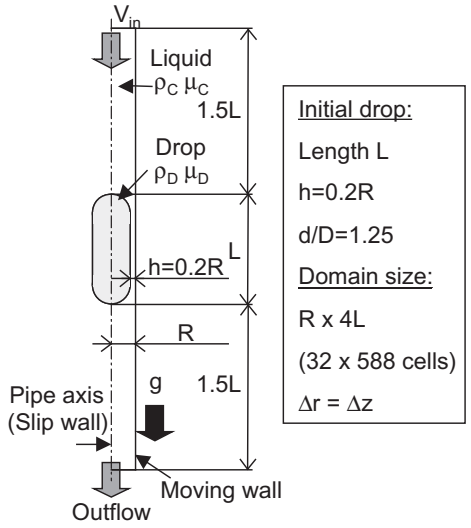

Fig. 14. Computational domain.

Numerical simulations with a higher spatial resolution, $\Delta r = \Delta z = R/64$, were carried out at several conditions to investigate the grid dependence. Terminal velocities predicted with the higher resolution agreed well with those predicted with the lower resolution. The relative error was about 1%. Hence the resolution of $\Delta r = R/32$ was sufficient for obtaining good predictions of V_T.

Another domain size, $(R, 7L)$, was also tested. The result confirmed that the influence of the top and bottom boundaries on predictions of V_T was negligibly small even with the domain size of $(R, 4L)$.

4.4. Comparisons

Comparisons between measured and predicted Fr are shown in Fig. 15. The simulations well reproduce the measured Fr for the wide range of dimensionless groups. The predicted Froude numbers are directly compared with the measured Fr in Fig. 16, which shows a very good agreement between them. Measured and predicted drop shapes are compared in Fig. 17. The predicted drop shapes also agree very well with the experiments.

The good agreement assures that the NSS can be used to investigate the effects of dimensionless groups on Fr.

5. Effects of ρ^* and μ^*

Simulations were carried out at several values of ρ^* to investigate the effects of ρ^* on Fr. The other dimensionless groups were set at $(\log M, Eo_D, \mu^*) = (-1.0, 50, 1.0)$ and $(\log M, Eo_D, \mu^*) = (-3.0, 20, 1.0)$. Predicted Froude numbers are plotted against ρ^* in Fig. 18, which clearly shows that ρ^* has no influence on Fr. Hence the coefficient c_3 in Eq. (28) must be zero, and the equation becomes a function of Re_D, Eo_D and μ^*:

$$Fr = \sqrt{\frac{c_1\left(\frac{h}{D}\right)^2}{c_2\left(\frac{h}{D}\right)^2 + \frac{H}{Re_D}}\left(1 + c_5\frac{D}{(R-h)}\frac{1}{Eo_D}\right)} \tag{51}$$

where

$$H = 1 + c_4\left(\frac{h}{R-h}\right)^2\mu^* \tag{52}$$

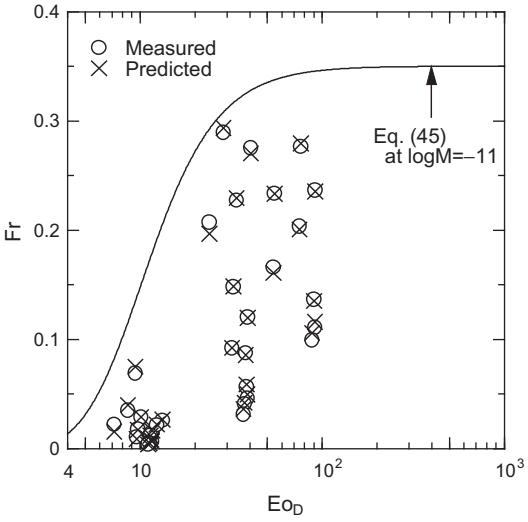

Fig. 15. Comparison of *Fr* in the Eo_D–*Fr* diagram.

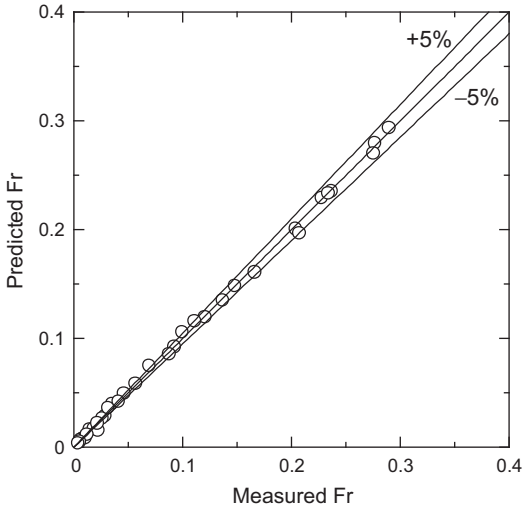

Fig. 16. Comparison between measured and predicted *Fr*.

The Froude number defined by Eq. (21) can be regarded as a combination of two dimensionless groups, $V_T/(gD)^{1/2}$ and ρ^*, i.e. $Fr = V_T/[(1-\rho^*)gD]^{1/2}$. Hence the dimensionless terminal velocity, $V_T/(gD)^{1/2}$ which is frequently used as the Froude number for a Taylor bubble, is proportional to $(1-\rho^*)^{1/2}$, i.e. $V_T/(gD)^{1/2} = (1-\rho^*)^{1/2} f(Re_D, Eo_D, \mu^*)$.

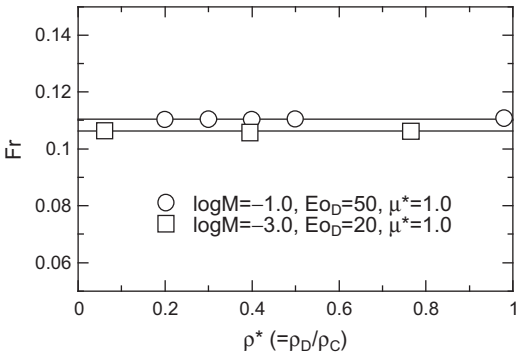

Fig. 18. Effect of ρ^* on *Fr*.

Comparing Eq. (51) with Eq. (29) gives the following expression

$$Fr = \sqrt{\frac{0.0089}{0.0725 + \frac{H}{Re_D}\left(1 - 0.11 Re_D^{0.33}\right)}\left(1 + \frac{41}{Eo_D^{1.96}}\right)^{-4.63}} \tag{53}$$

in which the effect of the drop viscosity is accounted for. As can be understood from Eq. (52), *H* should be a function of the viscosity ratio. Let us, therefore, deduce an empirical correlation of *H* in terms of μ^*.

Interface tracking simulations were carried out at various values of *M*, Eo_D and μ^*, i.e. $-8 < \log M < 4$, $9.8 < Eo_D < 200$ and $0 < \mu^* \leqslant 70$, to obtain the values of *H*. Solving Eq. (53) for *H* gives

$$H = \frac{Re_D}{1 - 0.11 Re_D^{0.33}}\left[\frac{0.0089}{Fr^2}\left(1 + \frac{41}{Eo_D^{1.96}}\right)^{-4.63} - 0.0725\right] \tag{54}$$

Substituting the numerical results into Eq. (54), we obtained the values of *H* as shown in Fig. 19. Since computed *H* scattered a lot due to the estimation error of Eq. (45), the values of *H* obtained at the same value of μ^* were averaged.

The functional form of *H* should satisfy the following requirements to reproduce the experimental fact: (1) $H(\mu^* = 0) = 1$, (2) *H* increases with μ^*, and (3) *H* becomes constant as $\mu^* \to \infty$. Referring to the numerical results and to the functional form of Eq. (3), we adopted the following functional form satisfying the above requirements:

$$H = \frac{1 + c_6 \mu^*}{1 + c_7 \mu^*} \tag{55}$$

where c_6 and c_7 are constants and $c_6 > c_7$. These constants were determined based on the data shown in Fig. 19, i.e. $c_6 = 1.9$ and $c_7 = 0.31$.

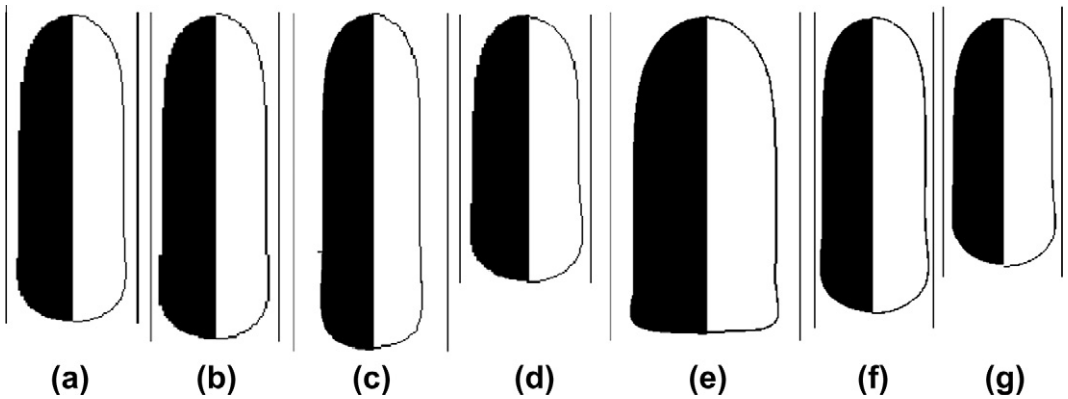

Fig. 17. Comparisons between measured and predicted shapes (left: measured, right: predicted). (a) ($\log M$, Eo_D, μ^*, d/D) = (−0.45, 12, 0.11, 1.24); (b) (−0.45, 12, 1.1, 1.27); (c) (−0.45, 39, 1.1, 1.07); (d) (−2.5, 10, 1.1, 1.19); (e) (−4.7, 26, 1.1, 1.01); (f) (−4.7, 8, 3.8, 1.34); (g) (−4.7, 8, 1.1, 1.24).

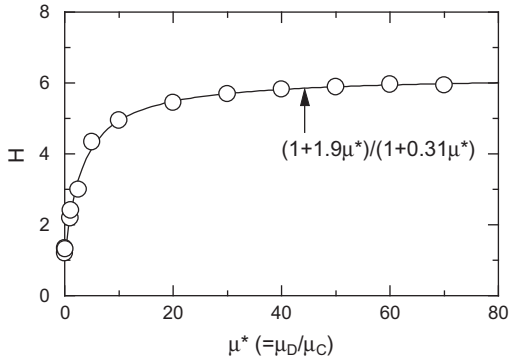

Fig. 19. Function *H*.

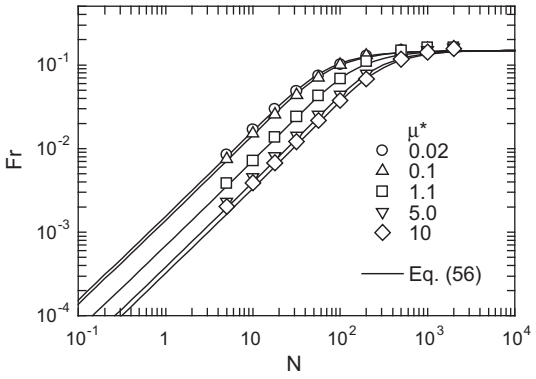

(a) $Eo_D = 10$

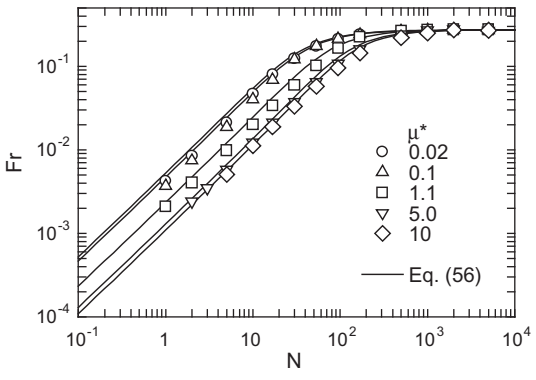

(b) $Eo_D = 20$

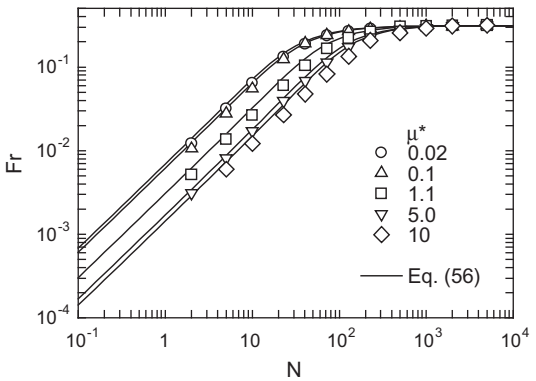

(c) $Eo_D = 30$

Fig. 20. Comparisons of *Fr* between predictions (symbols) and Eq. (56).

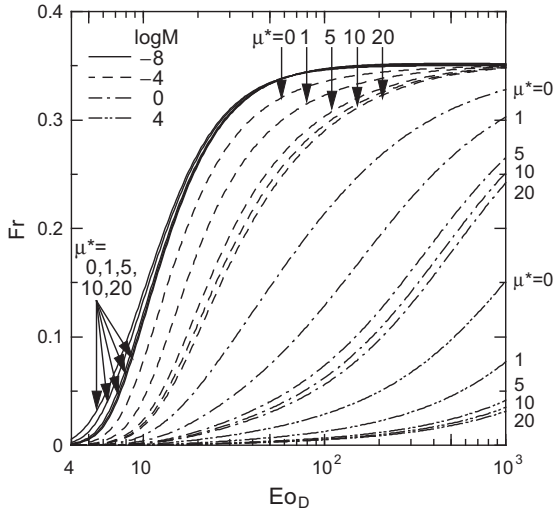

Fig. 21. Eq. (56) on the *Fr*–Eo_D plane.

6. Froude number correlation for Taylor drops

Substituting Eq. (55) and the constants, c_6 and c_7, into Eq. (53) gives the following correlation for Taylor drops:

$$Fr = \sqrt{\frac{0.0089\left(1+\frac{41}{Eo_D^{1.96}}\right)^{-4.63}}{0.0725+\frac{1}{Re_D}\left(\frac{1+1.9\mu^*}{1+0.31\mu^*}\right)\left(1-0.11Re_D^{0.33}\right)}} \tag{56}$$

This correlation is compared with the numerical predictions in Fig. 20. The correlation well reproduces the tendencies of *Fr*, i.e. *Fr* increases with *N* and Eo_D, while it decreases as μ^* increases. The agreement between Eq. (56) and the predictions is good. Hence the function of *H*, Eq. (55), well expresses the effects of μ^* on *Fr*. Fig. 21 shows *Fr* in terms of Eo_D, *M* and μ^*. Since Re_D is much larger than *H* for $Eo_D > 30$ and $\log M = -8$, the viscosity ratio does not have much influence on *Fr*. In this case, Eq. (44) can be used even if $\mu^* \neq 0$. *Fr* decreases with increasing μ^* for $\log M > -8$ even at high Froude numbers. The effects of μ^* on *Fr* become significant as *M* increases because of the decrease in Re_D.

The correlation is compared with the simulations and the experiments in Fig. 22, which includes 358, 34, 25 and 5 data of the simulations, the present experiments, Mandal's data and Goldsmith's data, respectively. The ranges of dimensionless groups

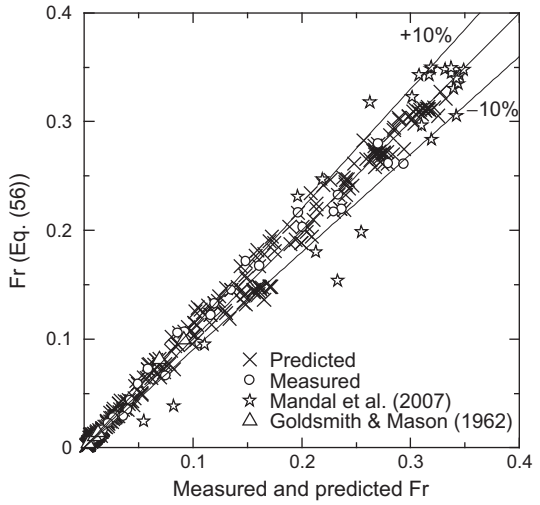

Fig. 22. Comparisons of *Fr* between measurements, predictions and Eq. (56).

are $4.8 < Eo_D < 228$, $1 < N < 14{,}700$, $-12 < \log M < 4$, $0.0 < \mu^* \leqslant 70$, and $0.002 < Re_D < 4960$. Most of the data obtained in this study lie within ±10% errors. The agreement between the correlation and Goldsmith's data is good. Though several Mandal's data do not agree with Eq. (56) due to the scatter of their data shown in Fig. 8, Eq. (56) well reproduces most of their data.

Eq. (56) reduces to Eq. (45) when $\mu^* = 0$. Hence Eq. (56) is applicable not only to Taylor drops but also to Taylor bubbles.

7. Conclusions

A correlation of Froude number, *Fr*, for Taylor drops rising through stagnant liquids in vertical pipes was proposed. The fundamental functional form of the correlation, $Fr = f(Re_D, Eo_D, \rho^*, \mu^*)$, was deduced by making use of a scaling analysis based on the field equations of two phases and the jump conditions at the interface, where Re_D is the drop Reynolds number, Eo_D the Eötvös number, ρ^* the density ratio and μ^* the viscosity ratio. Coefficients in the correlation were determined using experimental and numerical data. By taking the limits, $\rho^* \to 0$ and $\mu^* \to 0$, the correlation becomes applicable to Taylor bubbles in liquids. The coefficients relating with the effects of Re_D and Eo_D on *Fr* were, therefore, determined by making use of the knowledge on *Fr* of Taylor bubbles. Then, the effects of ρ^* and μ^* were investigated by using an interface tracking method. The simulation showed that ρ^* has no influence on *Fr*, whereas *Fr* monotonously decreases with increasing μ^*. The remaining terms in the correlation were determined based on the numerical predictions. As a result, the correlation, Eq. (56), was obtained. Comparisons between the proposed correlation, the measurements and the interface tracking simulations demonstrated that the correlation is applicable to Taylor drops for a wide range of the dimensionless groups, i.e., $4.8 < Eo_D < 228$, $1 < N < 14{,}700$, $-12 < \log M < 4$, $0 \leqslant \mu^* \leqslant 70$, $0.002 < Re_D < 4960$, and $d/D < 1.6$, where *N* is the inverse viscosity number and *M* the Morton number, *d* the sphere-volume equivalent drop diameter and *D* the pipe diameter.

Acknowledgements

This work has been supported by the Japan Society for the Promotion of Science (grant-in-aid for scientific research (B), No. 21360084). The authors would like to express our thanks to Mr. Yasuki Yoshikawa for his assistance in the experiments and simulations.

References

Brown, R.A.S., 1965. The mechanics of large gas bubbles in tubes. Can. J. Chem. Eng. 42, 217–223.
Collins, R., DeMoraes, F.F., Davidson, J.F., Harrison, D., 1978. The motion of a large gas bubble rising through liquid flowing in a tube. J. Fluid Mech. 89, 497–514.
Davies, R.M., Taylor, G.I., 1950. The mechanics of large bubbles rising through liquids in tubes. Proc.Roy. Soc. Lond. A 200, 375–390.
Dumitrescu, D.T., 1943. Stromung and Einer Luftbluse in Senkrechten rohr. Z. Angew. Math. Mech. 23, 139–149.
Goldsmith, H.L., Mason, S.G., 1962. The movement of single large bubbles in closed vertical tubes. J. Fluid Mech. 10, 42–58.
Griffith, P., Wallis, G.B., 1961. Two-phase slug flow. J. Heat Transfer 83, 307–320.
Harmathy, T.Z., 1960. Velocity of large drops and bubbles in media of infinite or restricted extent. AIChE J. 6, 281–288.
Hayashi, K., Tomiyama, A., 2007. Interface tracking simulation of bubbles and drops in complex geometries. Multiphase Sci. Tech. 19, 121–140.
Hayashi, K., Tomiyama, A., 2009. Drag correlation of fluid particles rising through stagnant liquids in vertical pipes at intermediate reynolds numbers. Chem. Eng. Sci. 64, 3019–3028.
Hayashi, K., Sou, A., Tomiyama, A., 2006. A volume tracking method based on non-uniform subcells and continuum surface force model using a local level set function. Comput. Fluid Dynam. J. 15, 225–232.
Hayashi, K., Kurimoto, R., Tomiyama, A., 2010. Dimensional analysis of terminal velocity of Taylor bubble in a vertical pipe. Multiphase Sci. Tech. 22 (3), 197–210.
Hirt, C.W., Nicholds, B.D., 1981. Volume of fluid (VOF) method for the dynamics of free boundaries. J. Comput. Phys. 39, 201–225.
Ishikawa, T., 1968. Kongou Ekinendo No Riron. Maruzen (in Japanese).
Joseph, D., 2003. Rise velocity of a spherical cap bubble. J. Fluid Mech. 488, 213–223.
Kurimoto, R., Hayashi, K., Tomiyama, A., 2010. Terminal velocity of a single drop in a vertical pipe in clean and fully-contaminated systems. In: Proc. 7th International Conference on Multiphase Flow, ICMF2010, Paper No. 4.2.3, 11pp.
Mandal, T.K., Das, G., Das, P.K., 2007. Prediction of rise velocity of a liquid Taylor bubbles in a vertical pipe. Phys. Fluids 19 (128109) 4pp.
Mandal, T.K., Das, G., Das, P.K., 2009. Liquid Taylor bubbles rising in a vertical column of a heavier liquid: an approximate analysis. J. Fluid Eng. 131 (011303) 7pp.
Nickens, H.V., Yannitell, D.W., 1987. The effects of surface tension and viscosity on the rise velocity of a large gas bubble in a closed, vertical liquid-filled tube. Int. J. Multiphase Flow 13 (1), 57–69.
Scardovelli, R., Zaleski, S., 2000. Direct numerical simulation of free-surface and interfacial flow. Ann. Rev. Fluid Mech. 31, 567–603.
Tomiyama, A., 2004. Drag, lift and virtual mass forces acting on a single bubble. In: Proc. 3rd Int. Sym. Two-Phase Flow Modelling and Experimentation, CD-ROM.
Tomiyama, A., Hirano, M., 1994. An improvement of the computational efficiency of the SOLA method. JSME Int. J., Ser. B 37, 821–826.
Tomiyama, A., Celata, G.P., Hosokawa, S., Yoshida, S., 2002. Terminal velocity of single bubbles in surface tension force dominant regime. Int. J. Multiphase Flow 28, 1497–1519.
Tung, K.W., Parlange, J.Y., 1976. Note on the motion of long bubbles in closed tubes – influence of surface tension. Acta Mech. 24, 313–317.
Viana, F., Pardo, R., Yanez, R., Trallero, J.L., Joseph, D., 2003. Universal correlation for the rise velocity of long gas bubbles in round pipes. J. Fluid Mech. 494, 379–398.
Wallis, G.B., 1969. One-Dimensional Two-Phase Flow. McGraw-Hill.
White, E.T., Beardmore, R.H., 1962. The velocity of rise of single cylindrical air bubbles through liquids contained in vertical tubes. Chem. Eng. Sci. 17, 351–361.